Title: Electrical resistivity, magnetism and electronic structure of the intermetallic 3d/4f Laves phase compounds ErNi2Mnx

Author: K. Balinski,T. V. Kuznetsova, E. G. Gerasimov, A. V. Protasov, V. V. Marchenkov, N. V. Mushnikov, Marcin Fijałkowski, Andrzej Ślebarski, Artur Chrobak i in.

Citation style: Balinski K., Kuznetsova T. V., Gerasimov E. G., Protasov A. V., Marchenkov V. V., Mushnikov N. V., Fijałkowski Marcin, Ślebarski Andrzej, Chrobak Artur i in. (2018). Electrical resistivity, magnetism and electronic structure of the intermetallic 3d/4f Laves phase compounds ErNi2Mnx. "AIP Advances " (vol. 8 (2018), Art. No. 105225), doi 10.1063/1.5048578

UNIWERSYTET ŚLĄSKI W KATOWICACH

Biblioteka Uniwersytetu Śląskiego

Ministerstwo Nauki i Szkolnictwa Wyższego

Electrical resistivity, magnetism and electronic structure of the intermetallic 3*d*/4*f* Laves phase compounds ErNi$_2$Mn$_x$

K. Balinski,[1,a] T. V. Kuznetsova,[2] E. G. Gerasimov,[2,3] A. V. Protasov,[2]
V. V. Marchenkov,[2,3] N. V. Mushnikov,[2,3] V. R. Galakhov,[2,3,4] V. V. Mesilov,[2]
S. N. Shamin,[2] V. S. Gaviko,[2] B. V. Senkovskiy,[5] M. Fijałkowski,[6]
L. Schneider,[1] A. Ślebarski,[6] A. Chrobak,[6] and K. Kuepper[1]

[1]*Osnabrück University, Department of Physics, 49076 Osnabrück, Germany*
[2]*M.N. Miheev Institute of Metal Physics, 620137 Yekaterinburg, Russia*
[3]*Ural Federal University, 620137 Yekaterinburg, Russia*
[4]*Ural State Mining University, 620137 Yekaterinburg, Russia*
[5]*II. Physikalisches Institut, Universität zu Köln, 50937 Köln, Germany*
[6]*University of Silesia, Department of Physics, 40-007 Katowice, Poland*

The non-stoichiometric intermetallic compounds RENi$_2$Mn$_x$ (RE = rare earth) with the cubic MgCu$_2$-type structure display a large variety of magnetic properties which is due to a complex interplay between the degrees of freedom of the 3*d* and 4*f* electrons and their interactions. We performed a comprehensive study of the electrical resistivity, magnetic properties and the electronic structure of ErNi$_2$Mn$_x$ (*x* =0, 0.25, 0.5, 0.75, 1, 1.25) compounds by employing a suitable set of complementary experimental approaches. We find an increase in electrical resistance compared to ErNi$_2$ upon Mn doping, the residual resistivity ratio decreases with increasing manganese content. The Curie temperature exhibits a sharp increase to around 50 K for Mn concentrations $x \geq 0.5$, whereas the saturation magnetization decreases with growing Mn content $x \geq 0.5$. Valence band X-ray photoelectron spectroscopy reveals an increasing intensity of Mn 3*d* states near Fermi energy in dependence of Mn concentration and Curie temperature. Resonant photoelectron spectroscopy of ErNi$_2$Mn$_{0.75}$ reveals that the photoemission decay channels dominate the valence band spectra across the Er N$_5$ and Mn L$_3$ X-ray absorption maxima, whereas the L$_3$VV Auger dictates the resonant valence band spectra close to and at the Ni L$_3$ X-ray absorption edge. © 2018 Author(s). All article content, except where otherwise noted, is licensed under a Creative Commons Attribution (CC BY) license (*http://creativecommons.org/licenses/by/4.0/*). https://doi.org/10.1063/1.5048578

I. INTRODUCTION

Rare earth (RE) and transition metal based compounds are of great scientific interest since the 1960s.[1,2] The combination of 4*f* lanthanides, which exhibit large magnetic moments including significant orbital contributions and anisotropy, with the more itinerant magnetism of 3*d* transition metals leads to a number of fascinating magnetic properties which are due to an intricate competition of the 4*f* − 4*f*, 4*f* − 3*d*, and 3*d* − 3*d* interactions in such compounds. The resulting magnetic properties are often difficult to predict by theoretical approaches. Hence, a careful investigation of the structural, electric, magnetic properties as well as the underlying electronic structure by means of a suitable set of experimental techniques is of most importance, also since a number of 3*d*/4*f* materials are interesting for different applications as strong permanent magnets,[3,4] hydrogen storage,[5,6] single molecule magnets,[7,8] or in the field of magneto calorimetry.[2,9] The intermetallic 3*d*/4*f* compounds

---

[a]Kamil Balinski: kbalinsk@uos.de

with the $MgCu_2$ -type face-centered cubic structure (Laves phase C15) are widely studied since they combine a relatively simple crystal structure and unique magnetic properties such as giant magnetostriction[10] and large magnetocaloric effect.[11,12]

It was accepted for a long time that the Laves phase compounds have no homogeneity range. A deviation from the stoichiometry usually leads to the formation of two-phase state. In the $RENi_2$ compounds with a small excess of nickel with respect to the stoichiometry, a cubic superstructure with doubled lattice parameter is formed, which is caused by ordering of vacancies in the rare-earth sublattice.[13] However, Wang et al. discovered that, similar to the binary $RENi_2$ and $REMn_2$, ternary $RENi_2Mn$ (RE = Tb, Dy, Ho, Er) alloys crystallize in the cubic $MgCu_2$ Laves phase ($Fd\bar{3}m$ space group).[14] Later it was reported that cobalt containing alloys $RECo_2Mn$ with the 1:3 stoichiometry also form the $MgCu_2$-type structure.[15–17] X-ray and neutron diffraction studies showed that the Mn atoms in Laves-phase structure of the $RENi_2Mn$ compounds partially occupy both the Ni (16d) and rare earth (8a) sites.[14,18] Such substitution assumes that the atomic ratio between the RE and $3d$ metals can be varied in some limits.

Magnetic properties and structure of the non-stoichiometric $RENi_2Mn_x$ alloys were studied for RE = Tb, Dy, Gd.[19–22] It was found that the $MgCu_2$-type structure persists up to the manganese content $x = 0.4$ for RE = Gd and up to $x = 1.25$ for RE = Tb. All the compounds are ferrimagnets below the Curie temperature T_C that is a non-monotonous function of Mn concentration. The values of T_C sharply increase with increasing x, reveal maximum around $x = 0.5$ and then slowly decrease. The maximum T_C values for $RENi_2Mn_x$ alloys amount to 120 K, 160 K and 190 K for RE = Dy, Tb and Gd, respectively. For RE = Er, a significant increase of T_C from 7 K in $ErNi_2$ up to 50 K in $ErNi_2Mn$ has been reported.[14,23]

It was long believed that Ni losses its magnetic moment in $RENi_2$.[24] However, accurate measurements indicate a small Ni moment induced from the RE side. Magnetic Compton profile studies reveal that in the $GdNi_2$ compound, the Ni magnetic moment as low as 0.23 μ_B is oriented antiparallel to the Gd moment.[25] For $RENi_2Mn_x$ alloys, the net magnetic moment gradually decreases with increasing x, which can be due to an increase in the magnetization of $3d$-sublattice. According to magnetization measurements,[21] neutron diffraction data,[18] and X-ray magnetic circular dichroism (XMCD) studies,[26,27] magnetic moment at the Ni site increases up to 0.6 μ_B, which is close to that of metallic nickel.

Thus, the $RENi_2Mn_x$ systems give the opportunity to gradually modify both magnetic moments and exchange interactions in the Laves phase compounds by changing in a wide range the manganese content. Here, we present a comprehensive study of the structural, electrical and magnetic properties $ErNi_2Mn_x$ ($x = 0, 0.25, 0.5, 0.75, 1,$ and 1.25) by means of X-ray diffraction, electrical transport measurements and magnetometry. Furthermore, we investigated the electronic structure by valence band X-ray photoelectron spectroscopy (XPS), and for the sample with $x = 0.75$ we employed complementary X-ray absorption spectroscopy (XAS) in combination with resonant X-ray photoelectron spectroscopy (ResPES) across the Mn $L_{2,3}$, Ni $L_{2,3}$ and Er $N_{4,5}$ edges.

II. EXPERIMENTAL DETAILS

The $ErNi_2Mn_x$ samples were produced at the M. N. Miheev Institute of Metal Physics, Ekaterinburg. The compounds were prepared by induction melting of the pure elements in an alumina crucible. The ingots were annealed at 870°C for 8 days. X-ray diffraction (XRD) analysis was carried out on powdered samples with the particle size 30–50 nm using a DRON-type diffractometer with Cr K_α radiation at room temperature. The XRD patterns were analyzed with help of the PowderCell 2.4 program. Temperature dependences of the initial ac magnetic susceptibility were measured with the system of compensated pick-up coils in a sinusoidal alternate magnetic field with the frequency 80 Hz and amplitude 300 A/m. The electroresistivity, FC-magnetization and magnetic hysteresis were measured by means of PPMS and SQUID techniques at the Dept. of Physics, University of Silesia in Katowice and at the Center of Collective Use, M.N. Miheev Institute of Metal Physics in Yekaterinburg. X-ray photoemission spectra (XPS) were recorded with the samples at room temperature at the Department of Physics at the University of Osnabrück. For the measurements, a PHI 5600ci spectrometer was used. The excitation source was a monochromatic Al K_α

anode with excitation energy of 1486.6 eV, and the overall resolution was 0.4 eV. Samples were cleaved in a preparation chamber in situ under UHV conditions ($\sim 1 \cdot 10^{-8}$ mbar), the pressure in the main chamber was kept below $3 \cdot 10^{-9}$ mbar during the experiments. Resonant photoemission spectroscopy (ResPES) and X-ray absorption spectroscopy (XAS) across the Mn $L_{2,3}$, Ni $L_{2,3}$ and Er $N_{4,5}$ edges of $ErNi_2Mn_{0.75}$ were performed after cleaving the sample in situ at the Russian-German beamline at BESSY II (Berlin). XAS was recorded in the surface sensitive total electron yield (TEY) mode. All XAS spectra were normalized to the beam flux measured by a clean gold mesh.

III. RESULTS AND DISCUSSION

For the studied compounds $ErNi_2Mn_x$ with $0 \leq x \leq 1$, X-ray diffraction patterns at room temperature can be well described on the assumption of the only cubic Laves phase C15 which belongs to $Fd\bar{3}m$ space group. The compound with $x = 1.25$, in addition to the main C15 phase, contains appreciable amount of a phase with the cubic $F\bar{4}3m$ structure. We prepared also the composition with $x = 1.5$. According to X-ray diffraction data, the $ErNi_2Mn_{1.5}$ alloy consists of a single $F\bar{4}3m$ phase that can be considered as an ordered variant of the cubic C15 Laves phase structure.[18,19] Figure 1 displays the lattice parameter a of the C15 phase with respect to manganese concentration x which was determined from the corresponding X-ray diffraction patterns. The crystal lattice parameter in the $ErNi_2Mn_x$-system increases from 7.13 Å to 7.15 Å with increasing Mn content, which corresponds to a lattice constant change of $\sim 0.3\%$.

Metallic radii of Er, Mn and Ni atoms amount to 1.761, 1.37 and 1.25 Å, respectively. The ratio of Er to Ni metallic radii equals to 1.409 that is considerably higher than an "ideal" value of 1.225 characteristic of the most compact arrangement of hard spheres of the two sizes within the $MgCu_2$-type unit cell.[28] The Ni–Ni distance in the $ErNi_2$ lattice equals to $\left(\sqrt{2}/4\right) \cdot a = 2.521$ Å, the value is very close to the doubled Ni metallic radius. Therefore, one may expect that growth of the lattice parameter in the course of addition of manganese to $ErNi_2$ is mainly caused by substitution of Ni by Mn atoms having larger size. At the same time, the Er–Ni distance in the $ErNi_2$ lattice amounts to $\left(\sqrt{11}/8\right) \cdot a = 2.521$ Å and appears to be slightly lower than the sum of the Er and Ni metallic radii. As a result, substitution of smaller Mn atoms for larger Er should lead to decrease of the lattice parameter. A competition of these two factors leads to monotoneous although very moderate growth of the lattice parameter with increasing x. It should be noted that for the RE atoms with larger metallic radii (Gd, Tb), a non-monotoneous concentration dependence of the lattice parameter of $RENi_2Mn_x$ was observed.[19,21]
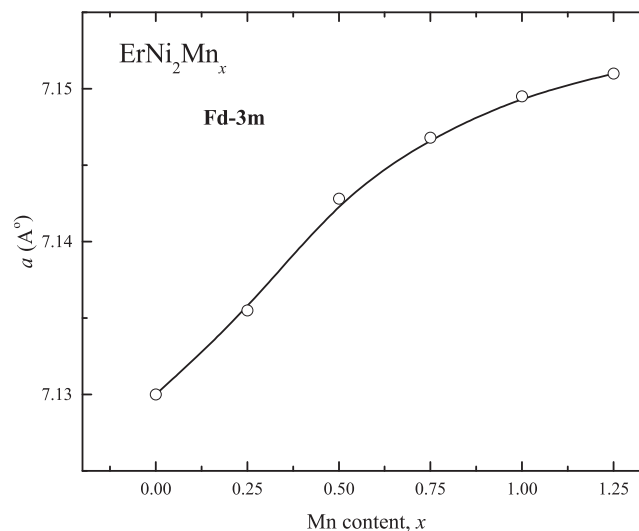

FIG. 1. Lattice parameter of $ErNi_2Mn_x$ as function of Mn content.

Addition of manganese strongly influences the conductivity of the compounds. The Fig. 2a) shows the residual resistivity ratio RRR (*i.e.* the ratio of resistivity at room temperature and at 4.2 K) of $ErNi_2Mn_x$ with respect to the Mn content. The results indicate that with higher Mn concentration more impurity in the system is build in. With no manganese, $ErNi_2$ shows a ratio of RRR $\approx$ 1.81 and with doping of Mn the ratio is continuously decreasing where it decreases down to 1.01 at $x = 1.25$. $ErNi_2$ exhibits a metallic type dependence of the resistivity as function of temperature (also cf. Fig. 2b)), the resistivity drops ~45% from room temperature to 4.2 K. Doping with Mn leads to a much lower temperature dependence of the electrical resistivity. For Mn concentrations $x \geq 0.75$ the resistivity can be considered as being independent of T. The changes of resistivity behavior can be explained by the impurity model. As seen from Fig. 2b), the resistivity increases around 4 times at 4.2 K and about 2.2 times at room temperature with Mn doping, leading to RRR decreasing (Fig. 2a)). In contrast, $DyNi_2Mn_x$ shows an increase in electrical resistivity up to $x = 0.5$ before dropping to almost linearly to a value of around $1.69 \cdot 10^{-4}$ Ohm·cm at $x = 1.25$,[22] which is exactly the (nearly temperature independent) result for $ErNi_2Mn_x$ at $x = 1.25$.

Turning to the magnetic properties of $ErNi_2Mn_x$ Fig. 3a) presents the zero field cooled (ZFC) and field cooled (FC) magnetization versus temperature ($M(T)$) curves of $ErNi_2Mn_x$ taken in an external magnetic field of 100 Oe in a temperature range of 2 – 75 K. The ZFC and FC curves
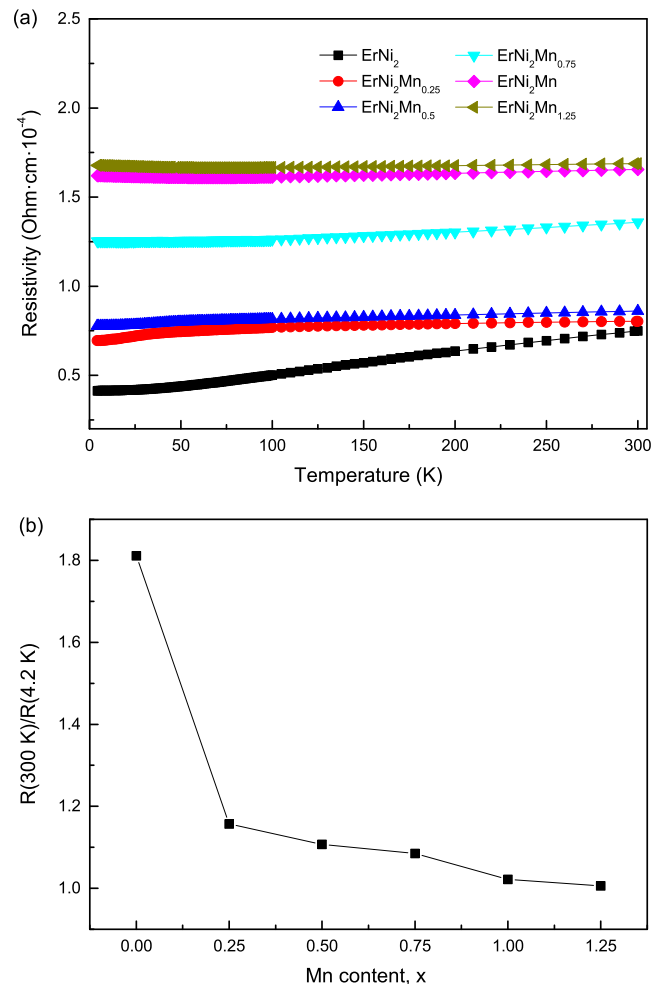

FIG. 2. (a) Concentration dependence of the residual-resistivity ratio of $ErNi_2Mn_x$ at 300 K/4.2 K. (b) Temperature dependence of the electrical resistance in a range from 4.2 K to 300 K.
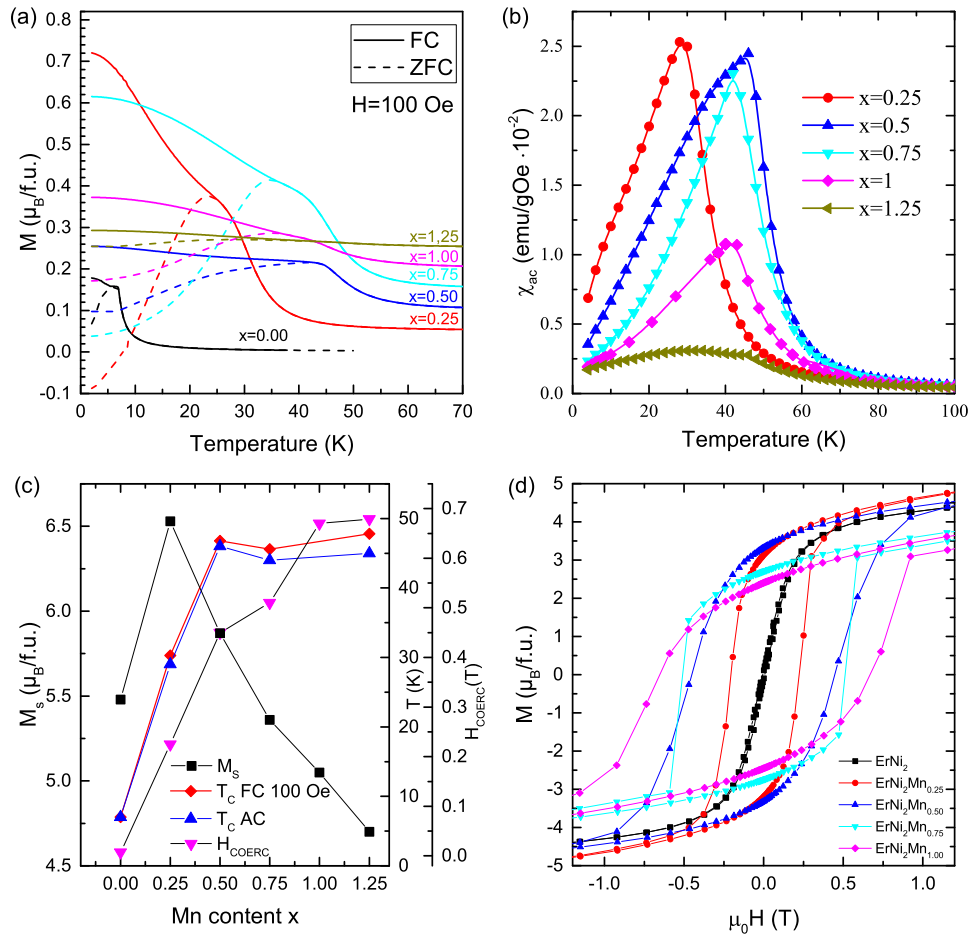
FIG. 3. (a) Zero-field - cooled (ZFC) and field cooled (FC) M(T)-curves recorded in a field of 100 Oe. (b) Magnetic susceptibility. (c) Saturation magnetization M_S (squares), Curie temperatures T_C, extracted from field cooled $M(T)$ curves performed at $H = 100$ Oe (Rhombus) and AC magnetic susceptibility (triangle) measurements of ErNi$_2$Mn$_x$ as function of Mn concentration x. (d) $M(H)$-hysteresis loops taken at $T = 2$ K. (right).

show bifurcations between 5.5 K (ErNi$_2$) and 43 K ($x = 0.5$). The FC magnetization increases with decreasing temperature, indicating ferromagnetic interactions in all samples. The FC magnetization increases rapidly for ErNi$_2$Mn$_{0.25}$ whereas it is almost flat for ErNi$_2$Mn$_{1.25}$. The ZFC magnetization decreases from the bifurcation for all samples. Such difference between ZFC and FC has been associated with different magnetic domain wall motion.[14] For the ZFC process, the magnetic domains are oriented in random directions, and magnetic fields lower than the coercivity field H_c are insufficient to move the domain walls. As the temperature increases, the coercivity decreases and the domain wall motion becomes easier which leads to the increase of both DC magnetization and AC magnetic susceptibility (in Fig. 3b)). In the FC regime, while cooling through the Curie temperature, the magnetic domains are oriented along the magnetic field direction, the domain walls move more easily which leads to higher magnetization.

In order to support the model explaining the difference between ZFC and FC curves, we measured magnetic hysteresis loops. Mn doping is found to lead to a strong increase of the coercive field at low temperature (Fig. 3c) and d)). The value of H_c increases up to almost 0.7 T for $x = 1$, 1.25, indicating that Mn doping changes the local anisotropy constants of the material. Even larger increase of the coercivity up to 1.3 T was observed earlier for the TbNi$_2$Mn$_x$ system.[19] Monotoneous increase in the coercivity with increasing the Mn content reflects the formation of magnetically heterogeneous state and gradual transition from a cubic to a local uniaxial anisotropy.

Also the occurrence of heterogeneous magnetic state as result of increasing Mn doping has to be considered as indicated by the obtained values for the saturation magnetization M_S at $T \approx 2$ K and $H = 70$ kOe (c.f. Fig. 3c)). For rare earth intermetallic compounds, the RE magnetic moment is usually close to its free-ion value $gJ\mu_B$, where g is the Lande factor and J is the quantum number of total angular momentum of RE^{3+} ion. However, the value of Erbium magnetic moment in $ErNi_2$ is much lower than 9 μ_B expected for the free Er^{3+}ion.[29] The magnetic moment is lowered down 5.5 μ_B because of two reasons. First, since the magnetic anisotropy is strong, the Er magnetic moments weakly deviate from the easy [111]-type directions of the cubic lattice in magnetic fields of the order of 7 T. Hence, for a random polycrystalline sample the magnetic moment amounts only 0.87 of its value for a single crystal. Second, since the energies of magnetocrystalline anisotropy and exchange interactions are comparable to each other in $ErNi_2$, the crystal electric field effect level scheme plays an important role in formation of Er magnetic moment. As seen from Fig. 3c) the value of M_S increases at an Mn concentration of $x = 0.25$. The increase can be caused by lowering crystal electric field effects, since the Mn alloying is accompanied by a considerable growth of the Curie temperature. Further doping with Mn leads to a decreasing saturation magnetization. $ErNi_2Mn_{1.25}$ exhibits an around 30% lower M_S compared to that measured for $ErNi_2Mn_{0.25}$. While in Ref. 14 $M_S = 4.5$ μ_B/f.u. for $ErNi_2Mn_{1.00}$ is reported, the saturation magnetization of $ErNi_2Mn_{1.00}$ in present work is 5.05 μ_B/f.u. Yu et al.[26] found the Ni magnetic moment of 0.6 μ_B and a very small magnetic moment at the Mn sites of $TbNi_2Mn$ by XMCD, which they associated with antiferromagnetic ordering of the Mn moments at the 8a and 16d sites. Then assuming antiparallel ordering of the Er and Ni moments in $ErNi_2Mn_{1.25}$, we estimate the Er moment value to be $5.1 + 2 \cdot 0.6 = 6.3$ μ_B that is much lower than the expected value $9 \cdot 0.87 = 7.83$ μ_B. This difference might be an indication of appearance of a local uniaxial anisotropy. When manganese statistically substituted a part of Erbium atoms at the 8a site, the symmetry of local crystal electric field at Er ions is lowered from cubic to uniaxial. A random orientation of magnetic anisotropy axes for different Er ions leads to lowering of the magnetic moment and increasing the coercivity.

Further, the Curie temperatures T_C were extracted from FC and magnetic susceptibility curves (AC) shown in Fig. 3b). We find an overall good agreement between the values obtained from the DC and AC curves, respectively. Determination of the values of T_C in case of FC measurements was done by obtaining the inflection points, while the T_C in AC curves is defined as their maximum (c.f. Fig. 3b)). While no differences in T_C occur at lower Mn concentrations ($x \geq 0.5$), the AC measurements indicate lower T_C values at higher concentrations. Since the inflection point is characteristic of the average Curie temperature, while the susceptibility maximum is associated with minimal transition temperature, the observed difference up to 2.8 K is due to an increase of the magnetic heterogeneity with increasing x. Wang et al.[14,23] estimate $T_C = 50$ (± 1) K for $ErNi_2Mn$ compound. The research done by Wang et al. in Ref. 23 indicates that the magnetic phase transition around the Curie temperature is of second order. We find a strong increase of T_C values for small Mn alloying, from around 7 K for $ErNi_2$ to almost 47 K for $ErNi_2Mn_{0.5}$. Higher Mn concentrations lead to slightly higher Curie temperatures, the maximum T_C of 48 K is obtained for $ErNi_2Mn_{1.25}$.

Another interesting approach to understand the magnetic behavior of $TbNi_2Mn$ is presented in Ref. 30 where the influence of the lattice parameter on T_C is drawn. The spacial separation of Mn atoms has a significant impact on the magnetic behavior of $TbNi_2Mn$ system. Our research is supporting the findings that appearance of Ni and Mn magnetic moments leads to strong enhancement of RE-$3d$ and $3d$–$3d$ exchange interactions in the $ErNi_2Mn_x$ compared to $ErNi_2$ and $ErMn_2$ system[19,30] and therefore, higher values of T_C can be expected. However, a modification of the magnetic state due to the volume changes is not observed. The lattice parameter of $ErNi_2Mn$ by Wang et al.[14] is estimated to be 7.126 Å, while the lattice parameter obtained in this work is 7.1495 Å, is slightly higher. However, there is no visible influence of T_C presented in Fig. 3 by the lattice parameter shown in Fig. 1. The changes observed in T_C can be accounted rather to the change of magnetic moments in the $3d$ subsystem than to the change of the lattice parameter. Hence, the Curie temperature of $ErNi_2Mn_x$ seems to be weakly altered by change in lattice parameter.

Next we want to discuss the electronic structure of the $ErNi_2Mn_x$ compounds. The off-resonance recorded XPS valence bands (c.f. Fig. 4) comprise of a distinct peak near Fermi Energy (E_F) with a
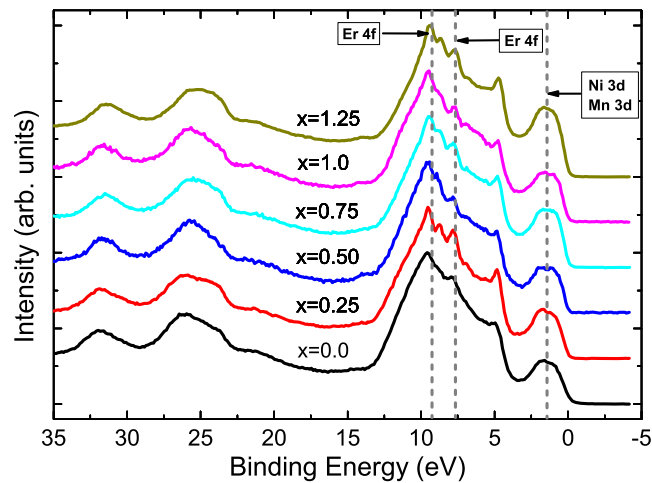
FIG. 4. XPS valence bands of ErNi$_2$Mn$_x$($x = 0, 0.25, 0.5, 0.75, 1, 1.25$) measured with a monochromatic Al K$_\alpha$ source ($E_{\mathrm{exc}} = 1486.6$ eV). The spectra are normalized to the maximum of the Er 4f states for comparison.

maximum in intensity around 1.7 eV. Besides some Er 5d states this region of the valence band is dominated by energetically overlapping Mn and Ni 3d states. The Er 4f multiplets, which also build up the total maximum in intensity at 9.6 eV from E_F, span the range between 4.8 eV and around 10 eV, Er 5$p_{3/2}$ and Er 5$p_{1/2}$ are localized around 25 and 32 eV, respectively. The 1.7 eV peak, and hence the concentration of Mn 3d and Ni 3d states near E_F show a maximum intensity for $x = 1.25$, where we also find the maximal Curie temperature of the overall ErNi$_2$Mn$_x$ series studies here. This might be associated with a change of the Er 5d – Mn/Ni 3d exchange interaction leading subsequently to a different density of states near E_F. A similar qualitative correlation has been reported for DyNi$_2$Mn$_x$[22] where the maximum intensity of transition metal 3d states and maximum T_C are found for $x = 0.5$.

In Fig. 5 we present the Mn L$_{2,3}$- and Ni L$_{2,3}$ -XAS spectra of ErNi$_2$Mn$_{0.75}$. The XAS recorded across the Ni $L_{2,3}$ – edges is rather similar to that of metallic nickel[31,32] (c.f. Fig. 5a)). There is a prominent feature located 6 eV above the Ni L_3 resonance (marked by arrows) in the spectra if Ni metal[31] and Ni@C nanoparticles,[32] which was associated with multiple scattering path of intermediate range for Ni metal.[31] In another work this feature has been attributed as being due to small amount of 3d^8 character (2$p^5$3d^9 final state) in the ground state via spd hybridization.[33] The somewhat different position of this feature in the spectrum of ErNi$_2$Mn$_{0.75}$ may indicate a different local and intermediate environment of the Ni atoms in ErNi$_2$Mn$_{0.75}$. Overall, the Ni electrons appear to be in a state close to that of metallic nickel. We find a different situation for manganese (Fig. 5b)). We compare the Mn $L_{2,3}$ edge spectrum of ErNi$_2$Mn$_{0.75}$ with those of metallic Mn, and diluted Mn in a Cu crystal and Ag crystal, respectively.[34] The latter spectrum can be almost perfectly described by atomic multiplet simulations, including the distinct features at the L_3 and L_2 edges.[34] Such features are also present for CuMn and ErNi$_2$Mn$_{0.75}$ (see arrows in Fig. 5b)), but with broader features and aL_2 intensity closer to that of metallic Mn, indicating that there is hybridization between the Mn atoms and likely the Er 4f/5d states for ErNi$_2$Mn$_{0.75}$. This result is different to results recently reported for TbNi$_2$Mn where atomic like multiplet spectra have been found for both, and Mn,[26] indicating that the Ni and Mn 3d electrons are much less localized in ErNi$_2$Mn$_x$ compared to TbNi$_2$Mn.

To gain deeper insight into the density of states we utilize element specific ResPES across the Er N$_{4,5}$ edges (4d to 4f transition) (c.f. Fig. 6a)), the Ni L$_{2,3}$ edges (2p to 3d transition) (Fig. 6b)), and the Mn L$_{2,3}$ edges, which are displayed in Fig. 6c). There is some energy dependence of the valence band photoemission spectra taken with excitation energies close to the Er N$_{4,5}$-edges. At $E_{exc} = 177$ eV the intensity around E$_F$ is enhanced as well as the region between ~3 eV to 7 eV. At higher excitation energies the feature between 7 eV and 11 eV is strongly resonating. The resonant features observed for Er are dispersionless and occur at constant binding energy. In case of Ni we
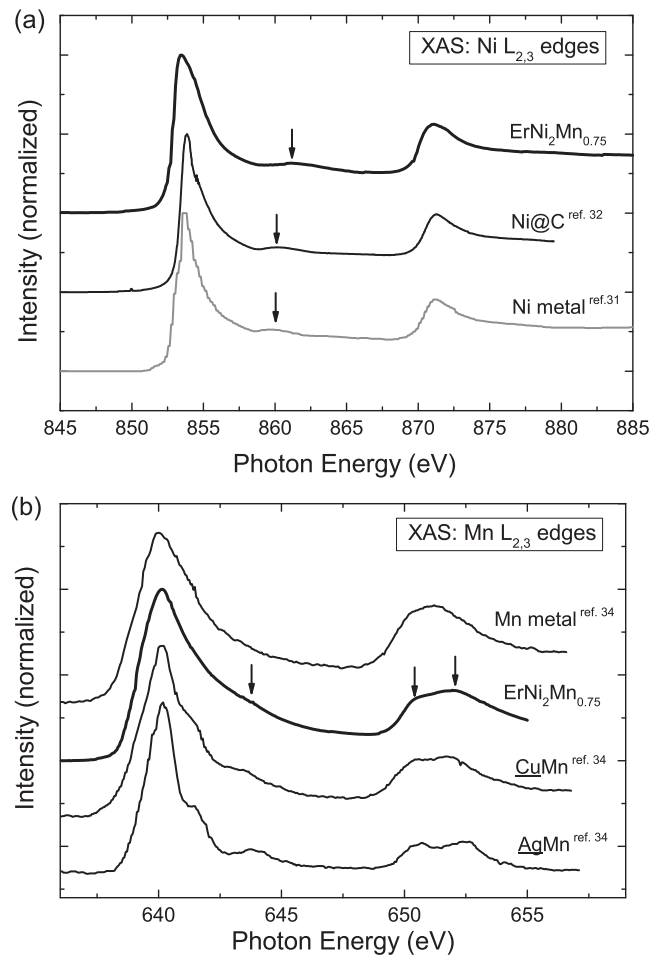
FIG. 5. (a) Ni $L_{2,3}$ edge-XAS of $ErNi_2Mn_{0.75}$ and the reference spectra of Ni@C nanoparticles[32] and metallic Ni, which has been extracted from Ref. [31]. (b) Mn $L_{2,3}$-XAS of $ErNi_2Mn_{0.75}$ along with reference spectra of metallic Mn, and Mn diluted in a Cu and Ag matrix, respectively. All three reference spectra have been extracted from Thole et al.[34]

observe a different resonance behavior at excitation energies close and across the Ni L_3 edge. We observe no specific enhancement of the excitation energy dependent valence band spectra which is constant at the binding energy scale. Close and above the Ni L_3 edge the L_3VV Auger emission, which is constant on the kinetic energy scale (assigned by the straight line as a guide to the eyes) is strongly resonating. Such an Auger final state is also called spectator, since the exciting electron is not any more participating the subsequent relaxation of the exciting state, and hence this is an incoherent process, indicating the itinerant character of the Ni 3d electrons.[35] We find a different situation for the resonant valence band spectra recorded close to and across the Mn L_3 edge (Fig. 6, c)). Here, the region close to Fermi energy and the region located around 5 eV binding energy show strong resonances close and at Mn L_3 resonance (E_{exc} = 640 eV), also the region between 7 and 10eV exhibits a strong enhancement in intensity which is constant with respect to the binding energy scale. Hence, the photoemission decay channels dominate the ResPES spectra across the Mn L_3 edge of $ErNi_2Mn_{0.75}$. Such processes occur coherently and under participation of the exciting electron, thus such electrons are also called participator. Since the decay via the photoemission channels is much faster (attosecond) time scale compared to the decay via Auger channels (∼1fs) the Auger peaks are completely or to large extend suppressed if the photoemission decay dominates. Similar behavior was interpreted by a high structural ordering of atoms in Heusler alloys.[36] This is also consistent with the potential antiferromagnetic alignment of the Mn sites discussed above, which requires a preferably equal occupation of the 16d and 8a sites in the crystal[26] Furthermore, in case of
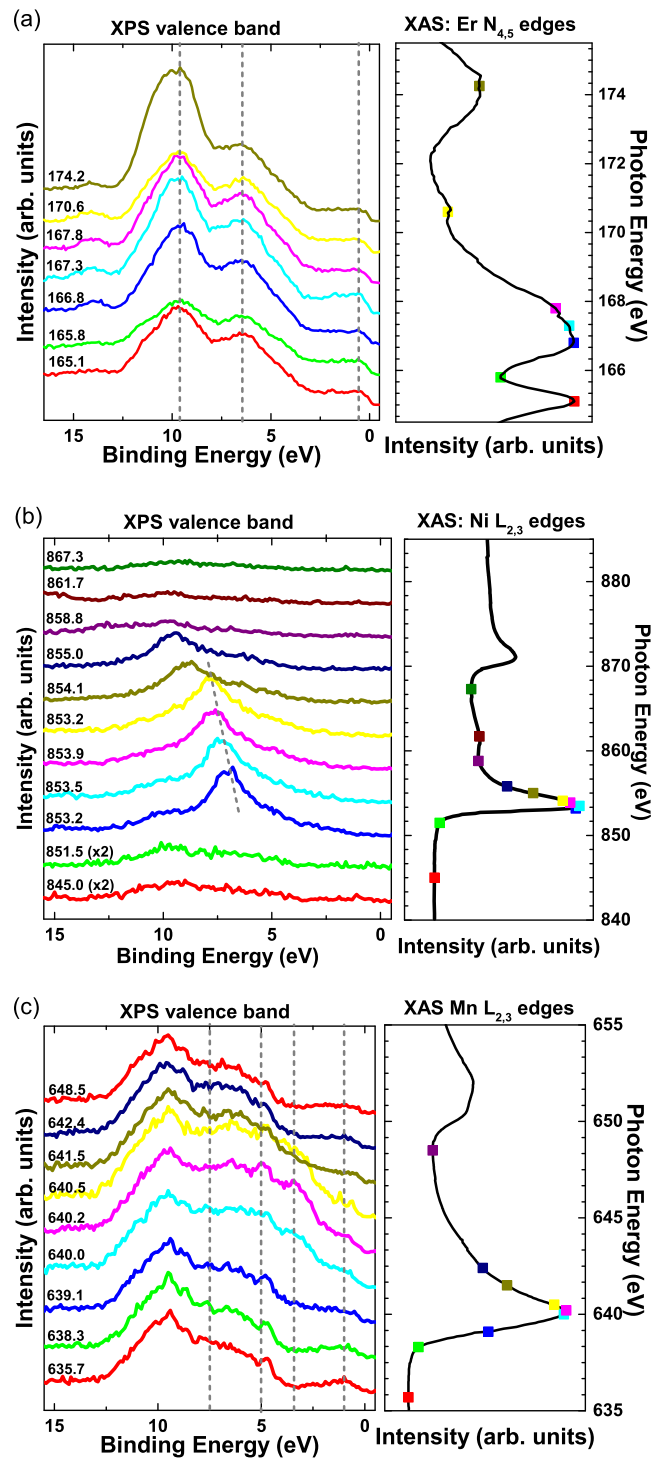
FIG. 6. (Left) Er $5d - 4f$ (a), Ni $2p - 3d$ (b), and Mn $2p - 3d$ (c) resonant photoemission spectra of ErNi$_2$Mn$_{0.75}$ performed at different excitation energies across the corresponding X-ray absorption edges (right). The corresponding excitation energies are indicated by solid squares in the XAS of equivalent color the resonant X-ray spectra are displayed. Excitation energies are also noted above the corresponding ResPES spectra.

ErNi$_2$Mn$_{0.75}$ the Mn $3d$ electrons appear to be partly localized close to E_F, but there seems to be also significant hybridization with Er $4f/5d$ states since the ResPES performed across the Er N and Mn L absorption edges show similar resonating behavior on a constant binding energy scale, whereas

the Ni 3d electrons exhibit a more itinerant character. These ResPES results are also in line with the conclusions drawn from the Mn $L_{2,3}$ and Ni $L_{2,3}$ XAS.

IV. CONCLUSIONS

We performed a comprehensive study of the structural, electric, and magnetic properties of $ErNi_2Mn_x$ ($x = 0, 0.25, 0.5, 0.75, 1, 1.25$). Doping of Mn into $ErNi_2$ leads to resistivity independency from the temperature in range of 2 K to 300 K for samples $x \geq 0.75$. The resistivity of $ErNi_2Mn_x$ shows a sharp drop at $x = 0.25$ at first, followed by a gradual increase up to a Mn concentration of $x = 1.25$, which is opposite to the result obtained at $DyNi_2Mn_x$. The $ErNi_2Mn_x$ system exhibits ferromagnetic behavior and an increase of T_C to a maximum of 48 K. The measurements indicate superparamagnetic domains and a predominantly antiferromagnetic ordering of the Mn sites for $x \geq 0.5$, leading to a decreased M_S which is in opposite to the electrical resistivity. A high coercive field observed at $x = 1$ and $x = 1.25$ suggests changes in the anisotropy constant caused by Mn doping. XPS valence band spectra showed correlation between T_C and Mn 3d orbitals at 1.7 eV which point to Er 5d and Mn/Ni 3d exchange interaction. While Ni is close to metallic state as XAS measurements indicate, the Mn $L_{2,3}$-XAS analysis of $ErNi_2Mn_{0.75}$ shows a hybridization of Mn states, possibly with Er 4f/5d states. Furthermore, the element specific ResPES confirmed the Mn 3d states to be partly hybridized with Er $4f/5d$ states and partly being localized near E_F whereas Ni $3d$ states are delocalized and show an itinerant character. To gain deeper insight into the complex magnetic properties of $ErNi_2Mn_x$, future studies employing polarized neutron reflectivity and scattering or X-ray magnetic circular dichroism would be highly desirable.

ACKNOWLEDGMENTS

[1] K. H. J. Buschow, Reports on Progress in Physics **40**, 1179 (1977).
[2] K. A. Gschneidner, V. K. Pecharsky, and A. O. Tsokol, Reports on Progress in Physics **68**, 1479 (2005).
[3] J. F. Herbst, J. J. Croat, F. E. Pinkerton, and W. B. Yelon, Phys. Rev. B **29**, 4176 (1984).
[4] S. Sugimoto, Journal of Physics D: Applied Physics **44**, 064001 (2011).
[5] B. Sakintuna, F. Lamari-Darkrim, and M. Hirscher, International Journal of Hydrogen Energy **32**, 1121 (2007).
[6] Q. Zhang, Z. Dong, and S. Xie, Journal of Alloys and Compounds **626**, 189 (2015).
[7] V. M. Mereacre, A. M. Ako, R. Clorac, W. Wernsdorfer, G. Filoti, J. Bartolome, C. E. Anson, and A. K. Powell, Journal of the American Chemical Society **129**, 9248 (2007).
[8] J.-B. Peng, Q.-C. Zhang, X.-J. Kong, Y.-Z. Zheng, Y.-P. Ren, L.-S. Long, R.-B. Huang, L.-S. Zheng, and Z. Zheng, Journal of the American Chemical Society **134**, 3314 (2012).
[9] E. Brück, Journal of Physics D: Applied Physics **38**, R381 (2005).
[10] G. Engdahl and I. Mayergoyz, *Handbook of Giant Magnetostrictive Materials*, Electromagnetism (Elsevier Science, 1999), ISBN 9780080533605, URL https://books.google.ru/books?id=wEgiiyfi5_kC.
[11] P. J. von Ranke, E. P. Nóbrega, I. G. de Oliveira, A. M. Gomes, and R. S. Sarthour, Phys. Rev. B **63**, 184406 (2001).
[12] J. Ćwik, T. Palewski, and K. Nenkov, Journal of Superconductivity and Novel Magnetism **26**, 183 (2013).
[13] E. Gratz, E. Goremychkin, M. Latroche, G. Hilscher, M. Rotter, H. Müller, A. Lindbaum, H. Michor, V. Paul-Boncour, and T. Fernandez-Diaz, Journal of Physics: Condensed Matter **11**, 7893 (1999).
[14] J. L. Wang, C. Marquina, M. R. Ibarra, and G. H. Wu, Phys. Rev. B **73**, 094436 (2006).
[15] B. Maji, K. G. Suresh, and A. K. Nigam, Journal of Magnetism and Magnetic Materials **322**, 2415 (2010).
[16] E. G. Gerasimov, N. V. Mushnikov, A. A. Inishev, P. B. Terentev, and V. S. Gaviko, Journal of Alloys and Compounds **680**, 359 (2016).
[17] C. Fang, J. Wang, F. Hong, W. D. Hutchison, M. F. M. Din, A. J. Studer, J. A. Kimpton, S. Dou, and Z. Cheng, Phys. Rev. B **96**, 064425 (2017).
[18] N. V. Mushnikov, V. S. Gaviko, J. Park, and A. N. Pirogov, Phys. Rev. B **79**, 184419 (2009).

[19] N. V. Mushnikov, V. S. Gaviko, E. G. Gerasimov, P. B. Terent'ev, and I. A. Tkach, The Physics of Metals and Metallography **110**, 210 (2010).

[20] N. V. Mushnikov, V. S. Gaviko, E. G. Gerasimov, P. B. Terentyev, I. A. Tkach, and A. V. Korolyov, in *Trends in Magnetism* (Trans Tech Publications, 2011), vol. 168 of Solid State Phenomena, pp. 200–203.

[21] E. G. Gerasimov, N. V. Mushnikov, P. B. Terentev, V. S. Gaviko, and A. A. Inishev, Journal of Alloys and Compounds **571**, 132 (2013).

[22] V. V. Marchenkov, N. V. Mushnikov, T. V. Kuznetsova, A. Buling, E. G. Gerasimov, V. S. Gaviko, V. I. Grebennikov, K. A. Fomina, H. W. Weber, C. Derks *et al.*, Journal of Physics: Conference Series **400**, 032050 (2012).

[23] J. L. Wang, S. J. Campbell, R. Zeng, S. X. Dou, and S. J. Kennedy, Journal of Applied Physics **109**, 07E304 (2011).

[24] K. Taylor, Advances in Physics **20**, 551 (1971).

[25] K. Yano, Y. Tanaka, I. Matsumoto, I. Umehara, K. Sato, H. Adachi, and H. Kawata, Journal of Physics: Condensed Matter **18**, 6891 (2006).

[26] D. Yu, M.-J. Huang, J. Wang, H.-C. Su, H.-J. Lin, C.-T. Chen, and S. Campbell, Journal of Magnetism and Magnetic Materials **370**, 32 (2014).

[27] T. V. Kuznetsova, V. I. Grebennikov, E. Gerasimov, and N. Mushnikov, Journal of Magnetism and Magnetic Materials **440**, 50 (2017), selected papers from the sixth Euro-Asian Symposium "Trends in Magnetism" (EASTMAG-2016).

[28] F. Stein, M. Palm, and G. Sauthoff, Intermetallics **12**, 713 (2004), intermetallic and Advanced Metallic Materials: A Symposium Dedicated to Dr. C. T. Liu, 3–6 March 2003, San Diego, CA, USA.

[29] M. R. Ibarra, J. I. Arnaudas, P. A. Algarabel, and A. del Moral, Journal of Magnetism and Magnetic Materials **46**, 167 (1984).

[30] J. Wang, S. J. Campbell, S. J. Kennedy, R. Zeng, S. X. Dou, and G. Wu, Journal of Physics: Condensed Matter **23** (2011).

[31] A. I. Nesvizhskii, A. L. Ankudinov, J. J. Rehr, and K. Baberschke, Phys. Rev. B **62**, 15295 (2000).

[32] V. Galakhov, S. N. Shamin, V. Mesilov, N. A. Ovechkina, M. Uymin, A. Yermakov, L. Schneider, K. Balinski, and B. Senkovskiy **118**, 30216 (2014).

[33] S. S. Dhesi, H. A. Dürr, G. van der Laan, E. Dudzik, and N. B. Brookes, Phys. Rev. B **60**, 12852 (1999).

[34] B. T. Thole, R. D. Cowan, G. A. Sawatzky, J. Fink, and J. C. Fuggle, Phys. Rev. B **31**, 6856 (1985).

[35] S. Hüfner, S.-H. Yang, B. S. Mun, C. S. Fadley, J. Schäfer, E. Rotenberg, and S. D. Kevan, Phys. Rev. B **61**, 12582 (2000).

[36] S. Wurmehl, G. H. Fecher, K. Kroth, F. Kronast, H. A. Dürr, Y. Takeda, Y. Saitoh, K. Kobayashi, H.-J. Lin, G. Schönhense *et al.*, Journal of Physics D: Applied Physics **39**, 803 (2006).